nature nanotechnology

LETTERS

PUBLISHED ONLINE: 4 JULY 2016 | DOI: 10.1038/NNANO.2016.111

Instantaneous ballistic velocity of suspended Brownian nanocrystals measured by upconversion nanothermometry

Carlos D. S. Brites[1], Xiaoji Xie[2], Mengistie L. Debasu[1], Xian Qin[3], Runfeng Chen[4], Wei Huang[2,4], João Rocha[5], Xiaogang Liu[3,6]* and Luís D. Carlos[1]*

Brownian motion is one of the most fascinating phenomena in nature[1,2]. Its conceptual implications have a profound impact in almost every field of science and even economics, from dissipative processes in thermodynamic systems[3,4], gene therapy in biomedical research[5], artificial motors[6] and galaxy formation[7] to the behaviour of stock prices[8]. However, despite extensive experimental investigations, the basic microscopic knowledge of prototypical systems such as colloidal particles in a fluid is still far from being complete. This is particularly the case for the measurement of the particles' instantaneous velocities, elusive due to the rapid random movements on extremely short timescales[9]. Here, we report the measurement of the instantaneous ballistic velocity of Brownian nanocrystals suspended in both aqueous and organic solvents. To achieve this, we develop a technique based on upconversion nanothermometry. We find that the population of excited electronic states in $NaYF_4$:Yb/Er nanocrystals at thermal equilibrium can be used for temperature mapping of the nanofluid with great thermal sensitivity (1.15% K^{-1} at 296 K) and a high spatial resolution (<1 μm). A distinct correlation between the heat flux in the nanofluid and the temporal evolution of Er^{3+} emission allows us to measure the instantaneous velocity of nanocrystals with different sizes and shapes.

In the prototypical Brownian colloidal system, the molecules of a fluid interact randomly both with each other and with the diluted colloidal particles, keeping them suspended and maintaining their spontaneous diffusion in arbitrary directions even in the absence of exterior disturbance. In spite of extensive experimental attempts, the measurement of the particles' instantaneous velocities remains a major challenge due to motion randomization in the so-called ballistic regime, namely at exceedingly short timescales (Fig. 1a)[10]. Optical tweezers are often used as a versatile tool to trap particles while simultaneously measuring their three-dimensional (3D) displacements with high temporal and spatial resolutions[11–13]. However, there are several fundamental limitations associated with this force-spectroscopy-based technique. First, it applies only to particles of several micrometres in diameter, requiring the construction of costly optical instruments with sensitive position detectors and high-power trapping lasers[10,11]. At the same time, the best-achieved temporal resolution is of the order of 10^{-8} s, whereas precise measurement of the instantaneous velocity in the ballistic regime would require values much smaller than the relaxation time of the particles (~10^{-10} s; Fig. 1b).

Luminescence spectroscopy is a simple but powerful technique for probing thermal transport in the micro- and nano-domains[14,15], such as in intracellular temperature monitoring[16,17]. By considering that the Brownian motion of a particle is governed by the properties of its local surroundings, such as the fluid viscosity and temperature[3,18], we demonstrate herein that this technique can be successfully used to investigate these environmental effects in great detail. In particular, we are able to quantify the instantaneous velocities of nanoparticles by means of upconversion nanothermometry. Our method encompasses the benefits of high spatial (<1 μm) and temperature resolution (~0.1 K) (ref. 19) without the need for overly diluted samples, with potential advantages arising from the inherent characteristics of upconversion nanocrystals such as the long-lived luminescence, large anti-Stokes shifts, high photochemical stability and high relative thermal sensitivity (1.15% K^{-1} at 296 K) of their luminescence spectra[20–24].

The experimental set-up is presented in Fig. 2a. A nanofluid container for upconversion nanocrystals is designed and coupled to a thermofoil heater on one side. The thermofoil heater generates a heat flow of 11.6×10^4 W m^{-2} in the nanofluid medium through the Joule effect (Supplementary Section V). A continuous wave laser diode (980 nm, 1.6×10^4 W m^{-2}) is then placed next to the container on a precisely controlled moving stage, allowing the nanofluids to be irradiated at different locations along the predesigned path of the heat flux. Subsequently a collimating lens collects the upconversion emission and the optical signal is guided to a fibre-coupled detector positioned in front of the nanofluid container.

As a proof-of-concept experiment, luminescent nanofluids containing $NaYF_4$:Yb/Er@$NaYF_4$ core–shell nanoparticles of ~23 nm in diameter were prepared and dispersed in water and chloroform in volume fractions (ϕ) of 0.0068–0.68% and 0.0085–0.85% (Supplementary Table 1), respectively. Note that the core–shell structure is adopted to minimize the emission loss induced by surface quenching. We have measured the luminescence spectral power distributions of the as-synthesized $NaYF_4$:Yb/Er@$NaYF_4$ nanoparticles dispersed in water (0.0068%) and chloroform (0.0085%) (Supplementary Figs 5–7 and Supplementary Table 2). To verify the temperature effect on upconversion emission, we heated an aqueous solution of the core–shell nanoparticles

[1]Department of Physics and CICECO, Aveiro Institute of Materials, Universidade de Aveiro, 3810-193 Aveiro, Portugal. [2]Key Laboratory of Flexible Electronics & Institute of Advanced Materials, Jiangsu National Synergetic Innovation Center for Advanced Materials, Nanjing Tech University, Nanjing 211816, China. [3]Institute of Materials Research and Engineering, Agency for Science, Technology and Research, 2 Fusionopolis Way, 138634 Singapore, Singapore. [4]Key Laboratory for Organic Electronics and Information Displays & Institute of Advanced Materials, Jiangsu National Synergetic Innovation Center for Advanced Materials, Nanjing University of Posts and Telecommunications, Nanjing 210023, China. [5]Departament of Chemistry and CICECO, Universidade de Aveiro, 3810-193 Aveiro, Portugal. [6]Department of Chemistry, National University of Singapore, 117543 Singapore, Singapore.
*e-mail: lcarlos@ua.pt; chmlx@nus.edu.sg

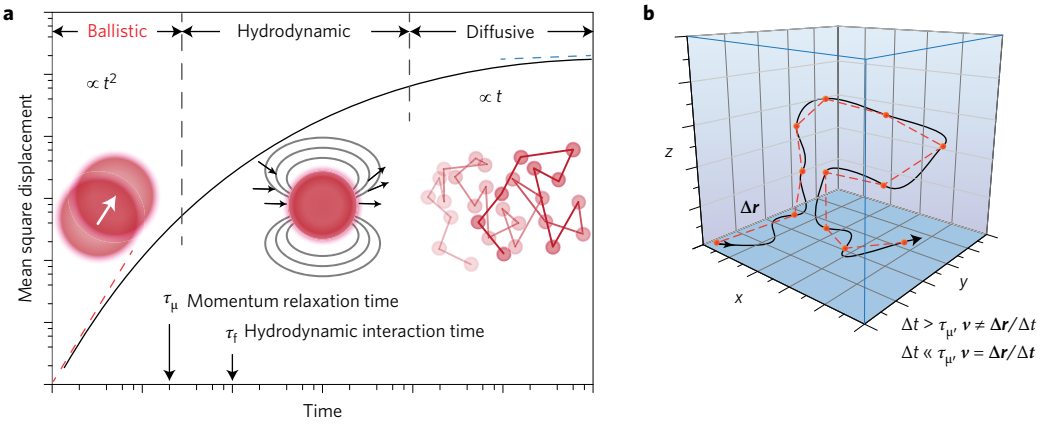

Figure 1 | Schematic characteristic timescales of Brownian motion in different regimes. a, Mean square displacement of a Brownian particle plotted against time. Note that at a very short timescale ($t \ll \tau_\mu$, where τ_μ is estimated to be 10^{-10} s for the water-based nanofluids in our study) the Brownian motion of the particle is in the ballistic regime and thus dominated by the particle's mass. In addition, the particle movement is subjected to the hydrodynamic memory effect of the liquid at an intermediate timescale ($\tau_\mu < t < \tau_f$). Over a much longer timescale ($t \gg \tau_f$, where τ_f is estimated to be $\sim 10^{-9}$ s for the water-based nanofluids) the Brownian motion is generally thought to be governed by particle diffusion. The dashed lines in red and blue show the expected behaviour of ballistic and diffusive Brownian motion, respectively. **b**, 3D trajectory of a single Brownian nanoparticle, indicating the effect of the temporal resolution on the measurement of the instantaneous velocity in the ballistic regime. The red dots denote the position of the nanoparticle and $\boldsymbol{r}$ is the displacement vector. The black curve is the real trajectory that the particle follows through space as a function of time. The trajectory measured at prolonged time intervals (red dashed line) is significantly different from the real trajectory. Thus, a stringent condition for the precise measurement of the nanoparticle's Brownian velocity is that the time interval Δt must be much smaller than τ_μ.

(0.0068%) and recorded their emission spectra in the range of 300–330 K on 980 nm excitation. Importantly, we found that the intensity ratio between the emission bands at 525 nm (I_H) and 545 nm (I_S) arising from the $^2H_{11/2} \rightarrow {}^4I_{15/2}$ and $^4S_{3/2} \rightarrow {}^4I_{15/2}$ transitions of Er^{3+}, respectively, increases with rising temperature. For example, when heated from 300 to 330 K the colloidal nanoparticles showed a marked increase in the emission intensity at 525 nm, accompanied by a concurrent decrease in the peak intensity at 545 nm (Fig. 2b). Notably, with each incremental increase in temperature from 300 to 330 K we observed clear trends of variation in the integrated I_H and I_S intensities (Fig. 2c).

The temperature sensitivity of the I_H/I_S intensity ratio (or thermometric parameter Δ) can be explained by considering the energy level structure of Er^{3+} (Fig. 2d). The $^2H_{11/2}$ level can be populated from the $^4S_{3/2}$ level by thermal excitation because of a small energy gap ($\sim 680\ cm^{-1}$) between the two energy levels. Importantly, the relative populations of the $^2H_{11/2}$ and $^4S_{3/2}$ levels in thermal equilibrium follows Boltzmann's distribution. Therefore, the thermometric parameter Δ can be expressed by[19,25]:

$$\Delta \equiv \frac{I_H}{I_S} = \frac{g_H A_H h\nu_H}{g_S A_S h\nu_S} \exp\left(-\frac{\Delta E}{k_B T}\right) \quad (1)$$

where g_i and A_i (i = H, S) are the degeneracies and the spontaneous emission rates of the $^2H_{11/2}$ and $^4S_{3/2}$ levels, respectively, ΔE is the energy gap between these two emitting levels, ν_i are the frequencies of the $^2H_{11/2} \rightarrow {}^4I_{15/2}$ and $^4S_{3/2} \rightarrow {}^4I_{15/2}$ transitions, h is Planck's constant, k_B is Boltzmann's constant and T represents the absolute temperature. The ΔE and ν_i values are measured by taking into account the barycentre of the $^2H_{11/2}$, $^4S_{3/2}$ and $^4I_{15/2}$ energy levels. Remarkably, when dispersed in water or chloroform the core–shell nanoparticles displayed a maximum relative thermal sensitivity S_r of 1.15% K^{-1} at 296 K, derived from $S_r = (1/\Delta)|\partial\Delta/\partial T|$ (refs 14, 19), regardless of the volume fraction (Supplementary Figs 8–10). These nanoparticle-based thermometers are extremely reliable, as evidenced by the consistent readings obtained after 10 consecutive cycles of experimentation (Supplementary Fig. 11).

To measure the temperature variation of the $NaYF_4$:Yb/Er@$NaYF_4$ nanoparticles induced by the heat flux in colloidal solutions the laser beam was switched on and focused at a given position, x_i, along the x direction, as shown in Fig. 2a. After turning on the heater, the upconversion emission spectra of Er^{3+} were recorded at different time intervals and compiled for analysis. For example, the blue curves shown in Fig. 3a,b depict the time-dependent temperature variation as recorded at position x_1 for highly diluted colloidal nanoparticles in water ($\phi = 0.0068\%$) and chloroform ($\phi = 0.0085\%$), respectively. Note that a critical time t_{0i} is determined from the onset of the change in emission induced by temperature variation. After ~300 s of heating the I_H/I_S intensity ratio remains essentially constant because the colloidal solutions are in thermal equilibrium.

In a further set of experiments, we constructed time-dependent temperature profiles of the nanofluids in both water and chloroform at different volume fractions by measuring the intensity ratio of I_H to I_S at six different positions (x_i = 0.2–0.9 cm; i = 1–6), as illustrated in Fig. 3a,b. Intriguingly, we obtained an excellent linear correlation between x_i and t_{0i}, as shown in Fig. 3c,d. The slope of the line plot from each dataset represents velocity v, which is the average instantaneous velocity of the nanoparticles illuminated by the laser beam. For highly diluted nanofluids we obtained velocity values of 0.31×10^{-3} m s^{-1} ($\phi = 0.0068\%$) and 0.16×10^{-3} m s^{-1} ($\phi = 0.0085\%$) in water and chloroform, respectively. Notably, these values are in good agreement with the instantaneous Brownian velocity determined for a single barium titanate microparticle in acetone (0.174×10^{-3} m s^{-1}) and also with the theoretical prediction ($\sim 10^{-3}$ m s^{-1}) for colloidal Au (~17 nm) and Al_2O_3 nanoparticles (~47 nm)[10,26–28]. Note that our results cannot be explained by the 1D transient heat conduction model (Supplementary Section VII). Moreover, the measured velocity is unlikely to be the thermophoretic velocity of the nanoparticles, because under our experimental conditions with a temperature gradient of 2,500 K m^{-1} the thermophoretic velocity was estimated to be 10^{-10} m s^{-1} (ref. 29), which is almost six orders of magnitude smaller than the velocity determined from our study.

Next, we address the question of whether the v value obtained above truly represents the instantaneous Brownian velocities of $NaYF_4$:Yb/Er@$NaYF_4$ nanoparticles. An important consideration is that the nanoparticles do not participate in the heat transfer

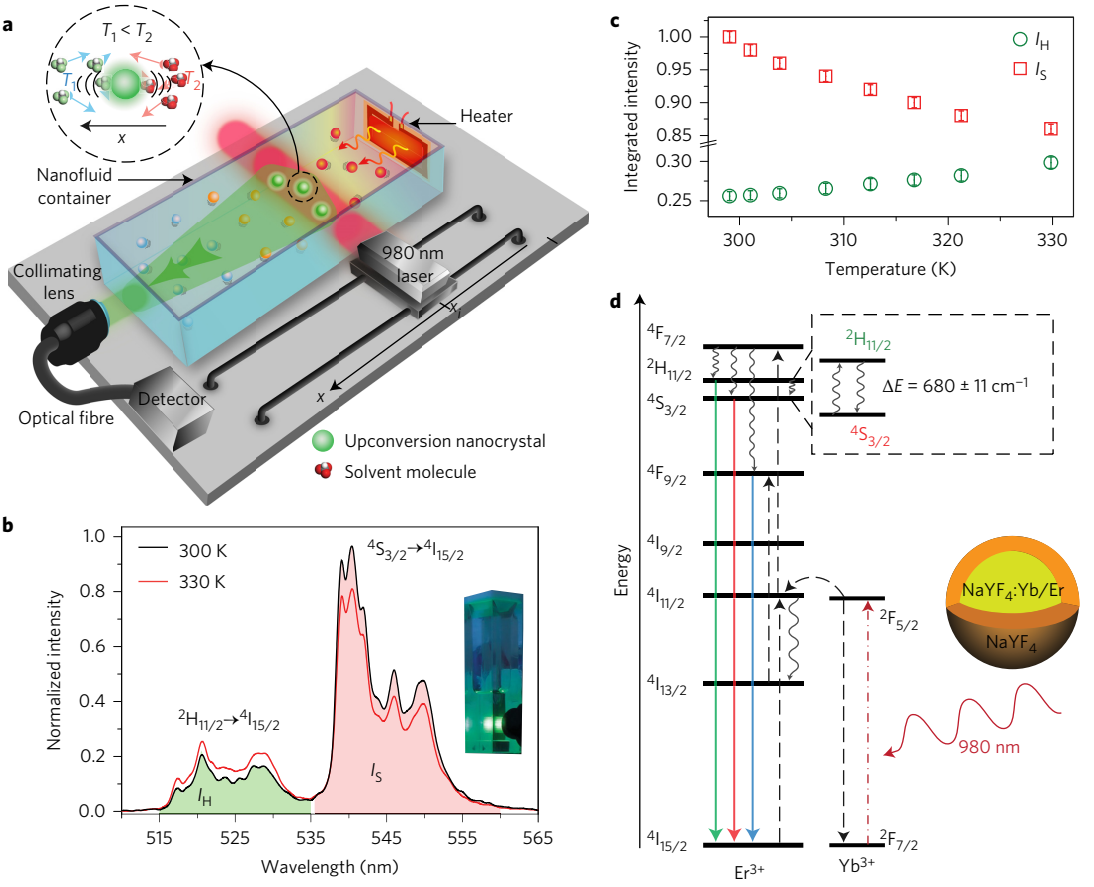

Figure 2 | Schematic of the experimental set-up and upconversion luminescence measurements of the $NaYF_4$:Yb/Er@$NaYF_4$ nanofluid. a, A collimating lens collects the upconversion emissions generated at different positions by moving a 980 nm laser along the *x* direction and the signals are guided to the detector by an optical fibre. The inset shows the solvent-mixing effect arising from the Brownian motion of the nanoparticle located at the interface between the cold (T_1) and hot (T_2) regions of the nanofluid. **b**, Emission spectra of the water-based nanofluid ($\phi = 0.0068\%$) recorded at 300 and 330 K. The spectra were normalized to Er^{3+} emission at 540 nm and 300 K. I_H and I_S correspond to the integrated intensities of $^2H_{11/2}\rightarrow{}^4I_{15/2}$ and $^4S_{3/2}\rightarrow{}^4I_{15/2}$ transitions of Er^{3+}, respectively. The inset shows a photograph of bright green emission of Er^{3+} with a luminous flux of $\sim 140 \times 10^{-3}$ lm (Supplementary Figs 5 and 7 and Supplementary Table 2). **c**, Temperature dependence of the integrated areas for I_H and I_S. Error bars show mean ± standard deviation. **d**, Proposed energy transfer mechanisms showing the upconversion processes dominated in the $NaYF_4$:Yb/Er@$NaYF_4$ nanoparticles under 980 nm excitation. The dashed-dotted, dashed, wavy and solid arrows represent photon excitation, energy transfer, multiphonon relaxation and emission processes, respectively.

process because the time ($\sim 10^{-12}$ s) required for thermalization of the nanoparticles is negligible when compared with the timescale of their Brownian motion (Supplementary Section VI). We attribute thermal conduction and nanoconvection (also known as the mixing effect of moving particles) to the heat transfer propagation in nanofluids when we impose a temperature gradient. The thermal conduction governs the collisions between solvent molecules and nanoconvection in turn governs the interactions between the solvent molecules and the nanoparticles. The increase in temperature increases the instantaneous Brownian velocity of the nanoparticles through nanoconvection, by which the nanoparticles push, drag and effectively mix the fluid molecules from regions of different temperature (Supplementary Section VII). On the basis of this nanoconvection effect, the timescale τ_S for pushing and dragging adjacent fluid molecules by the nanoparticles is approximately equal to the time required for a sound wave with a velocity v_s to travel a distance equivalent to the radius a of the nanoparticle: $\tau_S = a/v_s$ ($\tau_S = 7.7 \times 10^{-12}$ and 1.2×10^{-11} s for water and chloroform, respectively).

On the other hand, the timescale τ_f for acquiring a velocity by fluid molecules through the viscosity effect induced by the Brownian motion of the nanoparticle is defined as: $\tau_f = a^2\rho_p/\eta$, where ρ_p is the particle density, η is the viscosity of the fluid (10^{-3} and 0.563×10^{-3} Pa s for water and chloroform, respectively). This gives a viscous shear wave with a characteristic τ_f of 5.8×10^{-10} or 1.0×10^{-9} s for water or chloroform, respectively. In the case of water and chloroform, τ_f is much larger than τ_S ($\tau_f/\tau_S = 75$ and 88, respectively), that is, the time span for the fluid molecules to gain a velocity by the viscosity effect is much larger than the nanoconvection time required for reaching thermal equilibrium in the vicinity of the nanoparticles. We thus conclude that during the relaxation time, $\tau_\mu = 1.3 \times 10^{-10}$ s (for water) and $\tau_\mu = 2.3 \times 10^{-10}$ s (for chloroform), the particles are in thermal equilibrium with the solvent molecules, giving rise to changes in each particle's instantaneous Brownian velocity (Supplementary Section VI)[30]. We note that this same conclusion was assumed in a model proposed to account for the large enhancement of thermal conductivity in nanofluids and its strong temperature dependence[26].

As already discussed, the variation in the emission intensity of Er^{3+} corresponds to the change in the local temperature of the nanoparticles. If the kinetic energy of solvent molecules surrounding the nanoparticles changes in direct proportion with the temperature, then the changes in the instantaneous ballistic Brownian velocity of the nanoparticles can be discerned according to the temperature change. As the particle temperature change occurs on a timescale (thermalization time) much shorter than its relaxation time (Supplementary Section VI), the movement of the nanoparticles is probably in the ballistic regime, thus validating the measurements of the instantaneous velocity. Moreover, as the Boltzmann redistribution

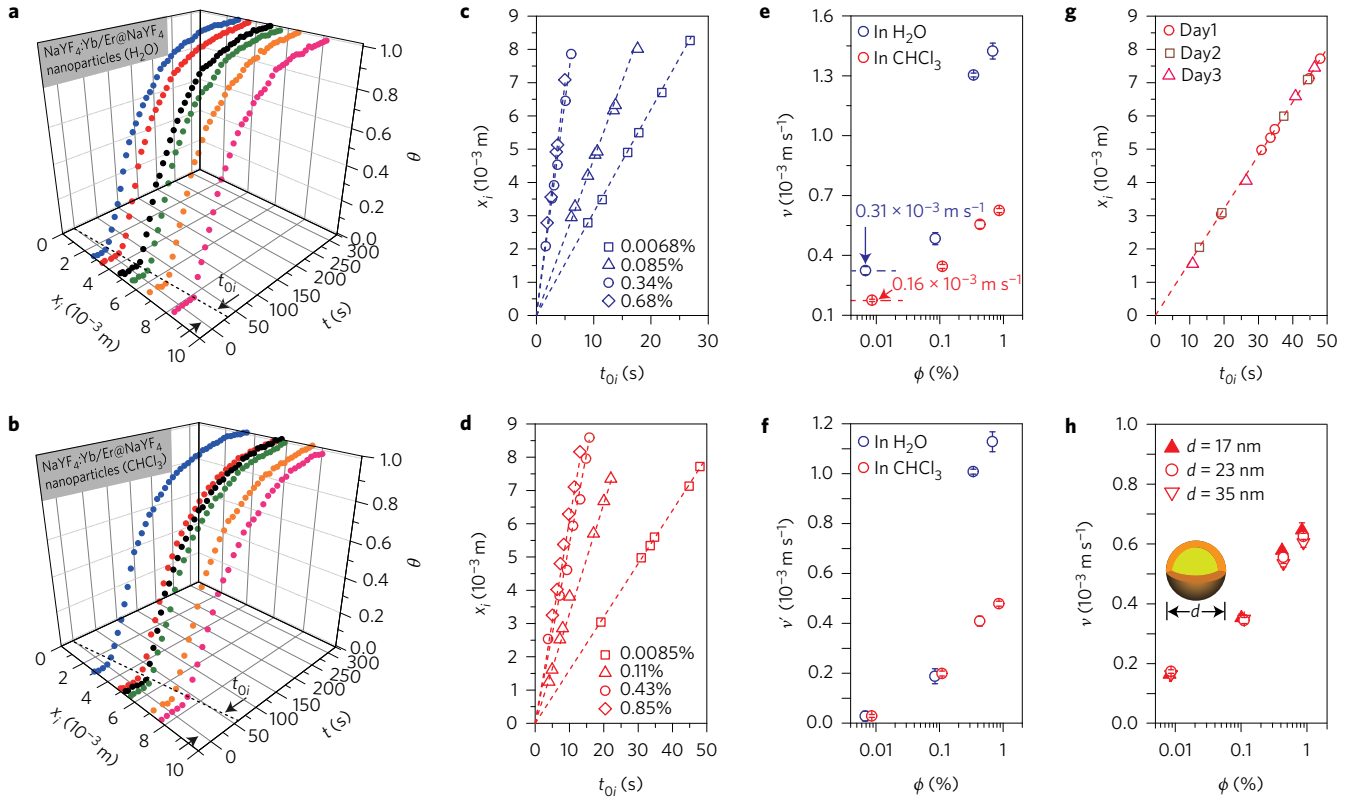

Figure 3 | Time-dependent temperature profile of the $NaYF_4$:Yb/Er@$NaYF_4$ nanofluid. a,b, Reduced temperature profiles of the nanoparticles dispersed in water (0.0068%; **a**) and chloroform ($CHCl_3$; 0.0085%; **b**), as measured by laser excitation from different positions x_i along the x direction (depicted in Fig. 2a). The dashed line refers to the critical time t_{0i} when the onset of change in ratio of I_H to I_S is observed due to temperature variation upon turning on the heater. **c,d**, The corresponding linear correlation ($r^2 > 0.994$) between x_i and t_{0i}, as measured in water (**c**) and chloroform (**d**) for the nanoparticles with different volume fractions, respectively. **e**, Measured velocities of the nanoparticles in water and chloroform as deduced from Fig. 3c,d. Error bars show mean ± s.d. **f**, The corresponding relative velocities of the nanoparticles in water and chloroform obtained by subtracting the solvent effect. **g**, The linear correlation data, generated on three different days, between x_i and t_{0i} from three batches of chloroform-based samples (0.0085%). **h**, Measured velocities of the core–shell nanoparticles of different sizes (17, 23 and 35 nm) recorded in chloroform. Note that the composition for the 17 nm nanoparticles is $NaYF_4$:Yb/Er/Gd@$NaYF_4$.

in the relative population of the $^2H_{11/2}$ and $^4S_{3/2}$ levels occurs on a timescale of ~10^{-15} s that is much shorter than that of particle thermalization[31], upconversion nanothermometry can be used to precisely determine the instantaneous Brownian velocity of nanoparticles.

An interesting observation is that the instantaneous velocity of the nanoparticle varies as a function of the volume fraction. As shown in Fig. 3e and Supplementary Fig. 23, the velocity value increased significantly for volume fractions higher than 0.2% for both nanofluids. The velocity dictated by the onset time (t_{0i}) increases with increasing volume fraction due to the increased heat transfer rates. Note that the dependence of the heat transfer rate on the particle volume fraction has been studied previously and the data have suggested that the heat transfer rate (or the effective thermal conductivity) increases as a function of the particle concentration[26]. Thus, for a given position x_i we observed a decrease of t_{0i} with increasing volume fraction, thereby leading to an increase in Brownian velocity (Supplementary Section VIII).

It is worth noting that the discrepancy between the measured values of the velocity in two different nanofluids can be ascribed to the solvent effect due to the momentum exchange of the solvent molecules on collision with the nanoparticles. To assess the solvent effect that could be expected, we further determined the relative velocity $v'(\phi)$ of the nanoparticles resulting from $v(\phi)$–v_F, where v_F denotes the Brownian velocity of the nanoparticles at infinite dilution in water (0.296×10^{-3} m s^{-1}) or chloroform (0.146×10^{-3} m s^{-1}) (Supplementary Fig. 17). Strikingly, almost identical relative velocities were obtained for diluted samples ($\phi < 0.2\%$) dispersed in water and chloroform (Fig. 3f).

The reproducibility of our approach was verified in chloroform by the evaluation of three batches of samples ($\phi = 0.0085\%$) on three different days. The experimental datasets compiled in Fig. 3g for all of the samples showed a strong positive linear association between x_i and t_{0i}. Another significant discovery is the independence of velocity from particle size for highly dilute samples, made evident by our control studies performed on three samples of different sizes (17, 23 and 35 nm) shown in Fig. 3h. Moreover, a subtle increase in the Brownian velocity with decreasing particle size is observed for high volume fractions of $\phi > 0.3\%$. Note that the enhancement of the thermal conductivity is inversely proportional to the particle size[26]. We thus can expect higher Brownian velocities to be obtained for smaller particles (Supplementary Section VIII).

The versatility of our upconversion nanothermometry-based approach is further exemplified by its ability to verify shape-independent Brownian motion of colloidal particles under highly diluted conditions. For simplicity, we synthesized water-dispersible $NaYF_4$:Yb/Er/Gd nanorods (313 × 76 nm) without the core–shell structure and constructed their time-dependent temperature profiles at different volume fractions (Fig. 4a and Supplementary Table 1). As anticipated, we obtained positive linear correlations between x_i and t_{0i} in all investigated cases (Fig. 4b). Intriguingly, the water-based nanofluids containing either spherical or rod-shaped nanocrystals at low volume fractions (<0.2%) revealed very similar velocity values

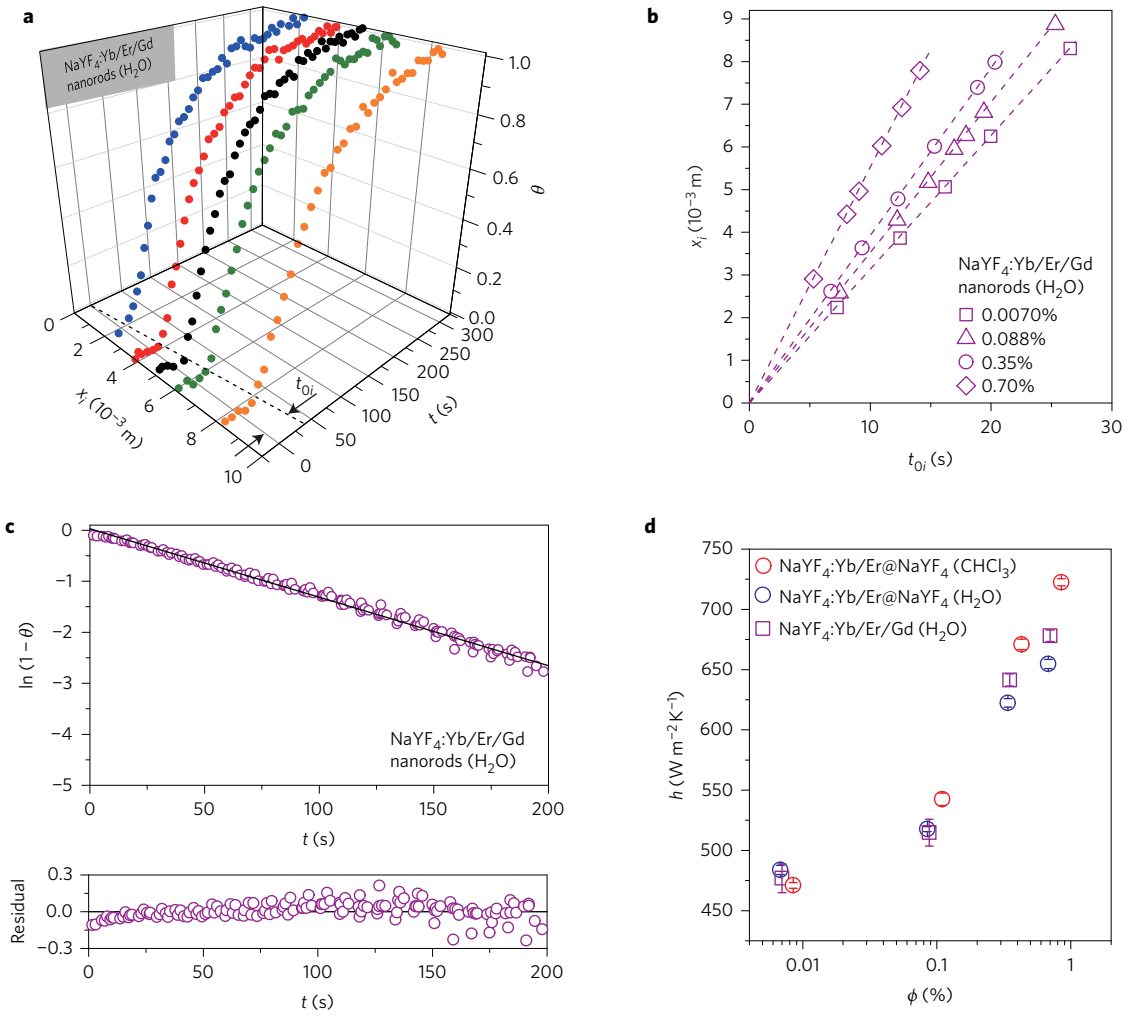

Figure 4 | Time-dependent temperature and heat-transfer-coefficient profiles of the fluid containing $NaYF_4$:Yb/Er/Gd nanorods. a, Reduced temperature profile of the nanorods dispersed in water (0.0068%) as recorded by laser excitation of the nanofluid at different positions x_i along the x direction (depicted in Fig. 2a). **b**, The corresponding linear correlations between x_i and t_{0i} as measured for water-based nanorod fluids with different volume fractions. **c**, Time-dependent reduced temperature profile (top) and its corresponding fitted residual (bottom) of the nanorod fluid ($r^2 > 0.981$), as deduced from Fig. 4a according to Newton's law of convective heat transfer. **d**, Convective heat transfer coefficients recorded in water and chloroform solutions containing $NaYF_4$:Yb/Er@$NaYF_4$ nanoparticles (23 nm) or $NaYF_4$:Yb/Er/Gd nanorods (313 × 76 nm). Error bars show mean ± s.d.

(Supplementary Table 6). This can be explained by the fact that under highly diluted conditions the particle–particle interactions are negligible and the enhancement of the thermal conductivity is marginal due to an insufficient amount of particle–solvent surface contact[26].

As an added benefit, our approach enables the measurement of the convective heat transfer coefficient, a characteristic constant that has been difficult to establish in convection systems due to the complexities of the fluid flow. Given the measured time-dependent development of the temperature profiles, convective heat transfer coefficient h of the nanorods (or nanoparticles) can be extrapolated (Fig. 4c,d and Supplementary Fig. 16) according to Newton's law of convective heat transfer[32]:

$$\theta(t) = 1 - \exp\left(-\frac{hA}{mc_p}t\right) \Leftrightarrow \ln(1-\theta) = -\frac{hA}{mc_p}t \qquad (2)$$

where A, m and c_p are the beam spot area, the mass of the fluid and its specific heat, respectively. The fitted heat transfer coefficient of the nanofluid containing nanorods ($\phi = 0.0068\%$) has an average value of 477 W m^{-2} K^{-1}, which is in good agreement with our estimate obtained from pure water (495 W m^{-2} K^{-1}, Supplementary Fig. 13) and the value given in the literature (458 W m^{-2} K^{-1}; ref. 33). Interestingly, we obtained similar h values for highly diluted nanoparticles and nanorods irrespective of the type of solvent used (Fig. 4d).

In summary, upconversion nanocrystals can be well dispersed into various solvents, yielding a versatile platform for investigating Brownian motion in the ballistic regime and related phenomena without the stringent constraints associated with optical tweezer-based techniques. Our results show that the instantaneous Brownian velocity depends on the volume fraction of the nanocrystals. However, at ultralow concentrations the velocity is independent of the crystal size and shape (or morphology) as well as the environment (aqueous or organic solvent) under study. Our technique should provide a more thorough understanding of the factors governing thermal conductivity, convective heat and mass transport in nanofluids. This possibility, albeit limited to fluids containing temperature-sensitive nanophosphors, may also have a profound impact on applications requiring nanofluidic systems with rapid and highly confined heat transfer performance.

Methods

Methods and any associated references are available in the online version of the paper.

Received 13 December 2015; accepted 20 May 2016; published online 4 July 2016

References

1. Einstein, A. Theoretical remarks on the Brownian motion. *Z. Elektrotech. Angew. P.* **13,** 41–42 (1907).
2. Frey, E. & Kroy, K. Brownian motion: a paradigm of soft matter and biological physics. *Ann. Phys.* **14,** 20–50 (2005).
3. Millen, J., Deesuwan, T., Barker, P. & Anders, J. Nanoscale temperature measurements using non-equilibrium Brownian dynamics of a levitated nanosphere. *Nature Nanotech.* **9,** 425–429 (2014).
4. Franosch, T. *et al.* Resonances arising from hydrodynamic memory in Brownian motion. *Nature* **478,** 85–88 (2011).
5. Chuck, A. S., Clarke, M. F. & Palsson, B. O. Retroviral infection is limited by Brownian motion. *Hum. Gene Ther.* **7,** 1527–1534 (1996).
6. Hutchison, J. A. *et al.* A surface-bound molecule that undergoes optically biased Brownian rotation. *Nature Nanotech.* **9,** 131–136 (2014).
7. Ossenkopf, V. Dust coagulation in dense molecular clouds: the formation of fluffy aggregates. *Astron. Astrophys.* **280,** 617–646 (1993).
8. Kou, S. G. A Jump-diffusion model for option pricing. *Manage. Sci.* **48,** 1086–1101 (2002).
9. Li, T. C. & Raizen, M. G. Brownian motion at short time scales. *Ann. Phys.* **525,** 281–295 (2013).
10. Kheifets, S., Simha, A., Melin, K., Li, T. C. & Raizen, M. G. Observation of Brownian motion in liquids at short times: instantaneous velocity and memory loss. *Science* **343,** 1493–1496 (2014).
11. Huang, R. X. *et al.* Direct observation of the full transition from ballistic to diffusive Brownian motion in a liquid. *Nature Phys.* **7,** 576–580 (2011).
12. Li, T. C., Kheifets, S. & Raizen, M. G. Millikelvin cooling of an optically trapped microsphere in vacuum. *Nature Phys.* **7,** 527–530 (2011).
13. Mor, F. M., Sienkiewicz, A., Forró, L. & Jeney, S. Upconversion particle as a local luminescent Brownian probe: a photonic force microscopy study. *ACS Photon.* **1,** 1251–1257 (2015).
14. Brites, C. D. S. *et al.* Thermometry at the nanoscale. *Nanoscale* **4,** 4799–4829 (2012).
15. Jaque, D. & Vetrone, F. Luminescence nanothermometry. *Nanoscale* **4,** 4301–4326 (2012).
16. Okabe, K. *et al.* Intracellular temperature mapping with a fluorescent polymeric thermometer and fluorescence lifetime imaging microscopy. *Nature Commun.* **3,** 705 (2012).
17. Kucsko, G. *et al.* Nanometre-scale thermometry in a living cell. *Nature* **500,** 54–58 (2013).
18. Kroy, K. Levitating nanoparticles: non-equilibrium nano-thermometry. *Nature Nanotech.* **9,** 415–417 (2014).
19. Wade, S. A., Collins, S. F. & Baxter, G. W. Fluorescence intensity ratio technique for optical fiber point temperature sensing. *J. Appl. Phys.* **94,** 4743–4756 (2003).
20. Bünzli, J. C. G. *et al.* Taking advantage of luminescent lanthanide ions. *Chem. Soc. Rev.* **34,** 1048–1077 (2005).
21. Vetrone, F. *et al.* Significance of Yb^{3+} concentration on the upconversion mechanisms in codoped Y_2O_3:Er^{3+},Yb^{3+} nanocrystals. *J. Appl. Phys.* **96,** 661–667 (2004).
22. Wang, F. *et al.* Simultaneous phase and size control of upconversion nanocrystals through lanthanide doping. *Nature* **463,** 1061–1065 (2010).
23. Gargas, D. J. *et al.* Engineering bright sub-10-nm upconverting nanocrystals for single-molecule imaging. *Nature Nanotech.* **9,** 300–305 (2014).
24. Deng, R. *et al.* Temporal full-colour tuning through non-steady-state upconversion. *Nature Nanotech.* **10,** 237–242 (2015).
25. Debasu, M. L. *et al.* All-in-one optical heater-thermometer nanoplatform operative from 300 to 2000 K based on Er^{3+} emission and blackbody radiation. *Adv. Mater.* **25,** 4868–4874 (2013).
26. Kumar, D. H. *et al.* Model for heat conduction in nanofluids. *Phys. Rev. Lett.* **93,** 144301–144304 (2004).
27. Kihm, K. D., Chon, C. H., Lee, J. S. & Choi, S. U. S. A new heat propagation velocity prevails over Brownian particle velocities in determining the thermal conductivities of nanofluids. *Nano. Res. Lett.* **6,** 361–369 (2011).
28. Prasher, R., Bhattacharya, P. & Phelan, P. E. Thermal conductivity of nanoscale colloidal solutions (nanofluids). *Phys. Rev. Lett.* **94,** 025901–025904 (2005).
29. Brenner, H. Self-thermophoresis and thermal self-diffusion in liquids and gases. *Phys. Rev. E* **82,** 036325–036341 (2010).
30. Li, C. H. & Peterson, G. P. The effect of particle size on the effective thermal conductivity of Al_2O_3-water nanofluids. *J. Appl. Phys.* **101,** 044312 (2007).
31. Lakowicz, J. R. *Principles of Fluorescence Spectroscopy* 2nd edn (Springer, 2013).
32. Incropera, F. P., DeWitt, D. P., Bergman, T. L. & Lavine, A. S. *Introduction to Heat Transfer* 5th edn (Wiley, 2006).
33. Rea, U., McKrell, T., Hu, L. W. & Buongiorno, J. Laminar convective heat transfer and viscous pressure loss of alumina–water and zirconia–water nanofluids. *Int. J. Heat Mass Tran.* **52,** 2042–2048 (2009).

Acknowledgements

We acknowledge V.S. Amaral for helpful discussion and Q. Sun for assistance with the nanorod synthesis. This work is supported by the CICECO-Aveiro Institute of Materials (FCT UID/CTM/50011/2013), financed by Portuguese funds through the FCT/MEC and when applicable co-financed by FEDER under the PT2020 Partnership Agreement. X.L. thanks the Agency for Science, Technology and Research (A*STAR) for support under contracts 122-PSE-0014 and 1231AFG028 (Singapore). W.H. is grateful for support from the National Basic Research Program of China (973, Grant 2015CB932200) and National Natural Science Foundation of China (61136003). C.D.S.B. and M.L.D. thank the FCT for postdoctoral research training (under grants SFRH/BPD/89003/2012 and SFRH/BPD/93884/2013).

Author contributions

C.D.S.B. and L.D.C. conceived the projects. C.D.S.B., L.D.C., J.R. and X.L. co-wrote the manuscript with input from other authors. C.D.S.B., X.X. and M.L.D. performed the experiments. X.Q., X.L., R.C., W.H. and L.D.C. provided input into the design of the experiments.

Additional information

Supplementary information is available in the online version of the paper. Reprints and permissions information is available online at www.nature.com/reprints. Correspondence and requests for materials should be addressed to X.L. and L.D.C.

Competing financial interests

The authors declare no competing financial interests.

Methods

Preparation of $NaYF_4$-based upconversion nanocrystals. $NaYF_4$-based core–shell nanoparticles and nanorods were synthesized by a standard co-precipitation or modified hydrothermal method according to ref. 22. Further experimental details are available in the Supplementary Information.

Operating procedure for temperature mapping. In a typical experiment, a Thorlabs quartz cuvette (CV10Q1400) was used as the container and filled with 0.50 ml of nanofluid. The temperature is increased at one side of the cuvette by thermal contact with a Kapton thermofoil heater (Minco). A continuous wave infrared laser diode (980 nm) is positioned next to the container and is controlled by a moving stage with a minimum step of 0.001 mm. The detection system consists of a collimating lens (74-UV, Ocean Optics), a USB-4000FL portable spectrometer (Ocean Optics) and a QP450-1-XSR optical fibre (Ocean Optics) that serves as a bridge between the lens and the spectrometer. During the excitation by the aforementioned continuous wave laser, the upconversion emissions generated by the lanthanide-doped nanocrystals at different positions are collected by collimating lens and the signals are subsequently guided to the detector through an optical fibre. Further experimental details and experimental data treatments are available in the Supplementary Information.